Article

Evolution Properties of a Partially Coherent Twisted Laguerre-Gaussian Pulsed Beam Propagating through Anisotropic Atmospheric Turbulence

Ying Xu [1], Yonggen Xu [1,*] and Tiejun Wang [2,3]

1 Department of Physics, School of Science, Xihua University, Chengdu 610039, China
2 State Key Laboratory of High Field Laser Physics, Shanghai Institute of Optics and Fine Mechanics, CAS Center for Excellence in Ultra-Intense Laser Science, Chinese Academy of Sciences, Shanghai 201800, China
3 Center of Materials Science and Optoelectronics Engineering, University of Chinese Academy of Sciences, Beijing 100049, China
* Correspondence: xuyonggen06@126.com

Abstract: Analytical expressions for the cross-spectral density matrix of a partially coherent twisted Laguerre-Gaussian pulsed (PCTLGP) beam in anisotropic atmospheric turbulence are derived based on the extended Huygens–Fresnel principle. Numerical results indicate that the atmospheric turbulence induces the degeneration of the spectral intensity distribution of the PCTLGP beam, and the PCTLGP beam also shows different evolution properties on propagation in weaker turbulence and stronger turbulence. The PCTLGP beam with a negative twisted factor exhibits an advantage over the Laguerre-Gaussian pulsed beam for reducing the atmospheric turbulence-induced degeneration, and this advantage is further strengthened with increasing the topological charge, mode order and absolute value of the twisted factor. In addition, we also find that the pulse duration will affect the spectral intensity of the PCTLGP beam in turbulence. This kind of beam will show potential application value in free-space optical communications and remote sensing.

Keywords: PCTLGP beam; twist phase; pulse duration; spectral intensity; anisotropic atmospheric turbulence

1. Introduction

Optical pulse has attracted enormous attention since the concept of the Gaussian Schell-Model pulsed (GSMP) beam was introduced by Paakkonen et al. [1,2]. Subsequently, the generation and propagation of various pulsed beams have been extensively studied [3–9]. In recent years, the partially coherent (PC) beams with a vortex phase carrying orbital angular momentum (OAM) have attracted considerable interest due to their various applications in free-space optical communications (FSOC), optical tweezers, astronomy [9–16], etc. The partially coherent Laguerre-Gaussian (PCLG) beam is a classical vortex beam that shows more obvious advantages in reducing the turbulence-induced scintillation [13–15]. A large number of studies have indicated that PCLG beams can be applied to the optical manipulation of Bose–Einstein condensates, optical imaging, biomedicine, quantum information coding and other fields [4,13–20]. Based on the merits of the OAM mode and the pulsed beam, the propagation of Laguerre-Gaussian pulsed (LGP) beams in the different channels have been investigated widely [4,21–23]. For examples, Martínez-Matos et al. studied the spatial pulse shaping of ultrashort Laguerre-Gaussian beams at the focal plane [21]. The time-varying of the pulse Laguerre-Gaussian beam propagating in free space has been analyzed by Gao et al. [22]. Li et al. investigated the probability distribution of OAM modes of the ultrashort LGP beam propagating through oceanic turbulence [23].

Many studies have been conducted on the propagation of PC beams through a turbulent atmosphere [6,7,9,13–15,20]. Researches have demonstrated that the anisotropic

atmospheric turbulence will seriously affect the characteristics of the beam in practical applications [7,13,15]. Therefore, reducing the influence of turbulence on beam propagation is necessary. The modulation of the vortex phase and twist phase is one of the important methods to effectively suppress the influence of turbulence [24–30]. Peng et al. introduced a PC twisted beam, named the twisted Laguerre-Gaussian Schell-model beam, which carries both the vortex phase and twist phase. The results show that the influence of atmospheric turbulence on the propagation characteristics for this beam can be effectively reduced by adjusting the twisted factor, topological charge and mode order [13,16,28–30].

However, to the best of our knowledge, the evolution properties of a partially coherent twisted Laguerre-Gaussian pulsed (PCTLGP) beam propagating through anisotropic atmospheric turbulence are still unreported so far. In this paper, we focus on the evolution of the spectral intensity distribution for the PCTLGP beam in anisotropic non-Kolmogorov turbulence. Analytical expressions for the cross-spectral density matrix (CSDM) of the PCTLGP beam propagating through the turbulence are derived, and numerical results are illustrated in detail. The results have reference value for the application of beams in FSOC and other fields.

2. Theoretical Formulation

In the source plane ($z = 0$), the statistical properties of the partially coherent Laguerre-Gaussian pulsed (PCLGP) beam at points $r_1 = (r_{1x}, r_{1y})$ and $r_2 = (r_{2x}, r_{2y})$, and at different instant times t_1 and t_2, can be characterized by a two-point two-time mutual coherent function matrix (MCFM), which is given by [7,9,13,15,20]:

$$\Gamma^{(0)}(r_1, r_2, 0; t_1, t_2) = \begin{bmatrix} \Gamma_{xx}^{(0)}(r_1, r_2, 0; t_1, t_2) & \Gamma_{xy}^{(0)}(r_1, r_2, 0; t_1, t_2) \\ \Gamma_{yx}^{(0)}(r_1, r_2, 0; t_1, t_2) & \Gamma_{yy}^{(0)}(r_1, r_2, 0; t_1, t_2) \end{bmatrix}$$

$$= \frac{1}{(2^{2n+l}n!)^2} \sum_{a_1=0}^{n} \sum_{b_1=0}^{l} \sum_{p_1=0}^{n} \sum_{q_1=0}^{l} (i^{b_1})^* i^{q_1} \binom{n}{a_1} \binom{l}{b_1} \binom{n}{p_1} \binom{l}{q_1}$$

$$\times H_{l+2a_1-b_1}\left(\frac{\sqrt{2}r_{1x}}{\sigma}\right) H_{l+2p_1-q_1}\left(\frac{\sqrt{2}r_{2x}}{\sigma}\right) H_{2n-2a_1+b_1}\left(\frac{\sqrt{2}r_{1y}}{\sigma}\right) H_{2n-2p_1+q_1}\left(\frac{\sqrt{2}r_{2y}}{\sigma}\right)$$

$$\times \exp\left[-\frac{r_1^2+r_2^2}{\sigma^2} - \frac{(r_1-r_2)^2}{2\delta^2}\right] \exp\left[-\frac{t_1^2+t_2^2}{2T_0^2} - \frac{(t_1-t_2)^2}{2T_c^2}\right]$$

$$\times \exp[-i\omega_0(t_2 - t_1)], \tag{1}$$

where $H(\cdot)$ being the Hermite polynomial, n and l denote the mode order and the topological charge, respectively. Their meanings are consistent throughout the paper. $\binom{n}{a_1}$, $\binom{l}{b_1}$, $\binom{n}{p_1}$ and $\binom{l}{q_1}$ are the binomial coefficients. σ and δ describe the waist width and the spatial coherence length, respectively. T_0 and T_c are the pulse duration and the temporal coherence length, respectively. ω_0 is the central angular frequency of the pulse. "*" describes the complex conjugate.

According to the Fourier-transform [9]

$$W_{\alpha\beta}(r_1, r_2, 0; \omega_1, \omega_2) = \iint \Gamma_{\alpha\beta}^{(0)}(r_1, r_2, 0; t_1, t_2) \exp[-i(\omega_2 t_2 - \omega_1 t_1)]dt_1 dt_2$$

$$(\alpha, \beta = x, y), \tag{2}$$

the two-point two-frequency CSDM of an PCLGP beam at $z = 0$ plane can be expressed as [7,13,20]:

$$W_{\alpha\beta}(r_1, r_2, 0; \omega_1, \omega_2) = \frac{T_0}{2\pi\Omega_0} \exp\left[-\frac{r_1^2 + r_2^2}{\sigma^2} - \frac{(r_1 - r_2)^2}{2\delta^2}\right]$$

$$\times \exp\left[-\frac{(\omega_1 - \omega_0)^2 + (\omega_2 - \omega_0)^2}{2\Omega_0^2} - \frac{(\omega_1 - \omega_2)^2}{2\Omega_c^2}\right]$$

$$\times \frac{1}{(2^{2n+l}n!)^2} \sum_{a_1=0}^{n} \sum_{b_1=0}^{l} \sum_{p_1=0}^{n} \sum_{q_1=0}^{l} (i^{b_1})^* i^{q_1} \binom{n}{a_1}\binom{l}{b_1}\binom{n}{p_1}\binom{l}{q_1}$$

$$\times H_{l+2a_1-b_1}\left(\frac{\sqrt{2}r_{1x}}{\sigma}\right) H_{l+2p_1-q_1}\left(\frac{\sqrt{2}r_{2x}}{\sigma}\right) H_{2n-2a_1+b_1}\left(\frac{\sqrt{2}r_{1y}}{\sigma}\right) H_{2n-2p_1+q_1}\left(\frac{\sqrt{2}r_{2y}}{\sigma}\right)$$

(3)

where $\Omega_0 = \sqrt{\frac{1}{T_0^2} + \frac{2}{T_c^2}}$ and $\Omega_c = \frac{\sqrt{T_0^2 + T_c^2}}{T_0^2}$ denote the spectral width and the spectral coherent width of the pulse, respectively.

According to the extended Huygens–Fresnel principle, the two-point two-frequency CSDM at the arbitrary two points $\rho_1 = (x_1, y_1)$ and $\rho_2 = (x_2, y_2)$ in the received plane ($z = L$) can be expressed as [7,9]:

$$W_{\alpha\beta}(\rho_1, \rho_2, L; \omega_1, \omega_2) = \frac{\omega_1\omega_2}{(2\pi cL)^2} \exp\left[-\frac{i(\omega_2 - \omega_1)L}{c}\right] \int \iiint d^2r_1 d^2r_2$$

$$\times W_{\alpha\beta}(r_1, r_2, 0; \omega_1, \omega_2)\langle\exp[\psi_1 + \psi_2^*]\rangle$$

$$\times \exp\left[-\frac{i\omega_1}{2cL}(r_1 - \rho_1)^2 + \frac{i\omega_2}{2cL}(r_2 - \rho_2)^2\right],$$

(4)

where L is the propagation distance, and c is the speed of light in a vacuum. $\langle\cdot\rangle$ denotes the ensemble average, and the turbulent factor $\langle\exp[\psi_1 + \psi_2^*]\rangle$ is given by [3,13,15,20]:

$$\langle\exp[\psi_1 + \psi_2^*]\rangle \approx \exp\left[-\frac{(\rho_1 - \rho_2)^2 + (\rho_1 - \rho_2)(r_1 - r_2) + (r_1 - r_2)^2}{\rho_0^2}\right],$$

(5)

where ρ_0 denotes the coherence length of a spherical wave propagating in turbulence and is given by [3,13,16]:

$$\rho_0 = \left[\frac{\pi^2 k^2 L}{3} \int_0^{\infty} \kappa^3 \Phi_n(\kappa) d\kappa\right]^{-1/2},$$

(6)

where $k = 2\pi/\lambda$, is the wave number, with λ as the wavelength. $\Phi_n(\kappa)$ represents the spatial power spectrum of the refractive-index fluctuations of anisotropic atmospheric turbulence with $\kappa = (\kappa_x, \kappa_y, \kappa_z)$ denoting the spatial wavenumber, and is given by [7,13]:

$$\Phi_n(\kappa) = \frac{A(\alpha)\widetilde{C}_n^2 \xi_x \xi_y}{\left(\xi_x^2\kappa_x^2 + \xi_y^2\kappa_y^2 + \kappa_z^2 + \kappa_0^2\right)^{\alpha/2}} \exp\left(-\frac{\xi_x^2\kappa_x^2 + \xi_y^2\kappa_y^2 + \kappa_z^2}{\kappa_m^2}\right)$$

$$(3 < \alpha < 4),$$

(7)

where α is the spectral power law, $\widetilde{C}_n^2$ is the generalized refractive structure constant with units $m^{3-\alpha}$. ξ_x and ξ_y are the anisotropic factors that can describe the asymmetry of turbulence cells. $A(\alpha) = \cos(\alpha\pi/2)\Gamma(\alpha-1)/(4\pi^2)$, $c(\alpha) = [2\pi A(\alpha)\Gamma(5/2-\alpha/2)/3]^{1/(\alpha-5)}$ with $\Gamma(\cdot)$ represents the Gamma function. κ_x, κ_y and κ_z are three components of the κ along the x, y and z directions. $\kappa_m = c(\alpha)/l_0$ and $\kappa_0 = 2\pi/L_0$. l_0 and L_0 are the turbulence inner and outer scales, respectively.

After the twist phase modulation is applied to PCLGP beam, with the setting $\omega_1 = \omega_2 = \omega$, the CSDM of a PCTLGP beam in the received plane can be obtained [7,9,13]:

$$
\begin{aligned}
W_{\alpha\beta}(\boldsymbol{\rho}_1, \boldsymbol{\rho}_2, L; \omega) = {} & \frac{\omega^2}{\left(2^{2n+l}\pi c L n!\right)^2} \frac{T_0}{8\pi\Omega_0} \exp\left[-\frac{(\omega-\omega_0)^2}{\Omega_0^2}\right] \\
& \times \int \iiint d^2\boldsymbol{r}_1 d^2\boldsymbol{r}_2 \sum_{a_1=0}^{n}\sum_{b_1=0}^{l}\sum_{p_1=0}^{n}\sum_{q_1=0}^{l} (i^{b_1})^* i^{q_1} \binom{n}{a_1}\binom{l}{b_1}\binom{n}{p_1}\binom{l}{q_1} \\
& \times H_{l+2a_1-b_1}\left(\frac{\sqrt{2}r_{1x}}{\sigma}\right) H_{l+2p_1-q_1}\left(\frac{\sqrt{2}r_{2x}}{\sigma}\right) H_{2n-2a_1+b_1}\left(\frac{\sqrt{2}r_{1y}}{\sigma}\right) H_{2n-2p_1+q_1}\left(\frac{\sqrt{2}r_{2y}}{\sigma}\right) \\
& \times \exp\left[-ik\eta\left(r_{1x}r_{2y} - r_{2x}r_{1y}\right)\right] \exp\left[-\frac{r_1^2+r_2^2}{\sigma^2} - \frac{(r_1-r_2)^2}{2\delta^2}\right] \\
& \times \langle \exp[\psi_1 + \psi_2^*]\rangle \exp\left[-\frac{i\omega}{2cL}(\boldsymbol{r}_1-\boldsymbol{\rho}_1)^2 + \frac{i\omega}{2cL}(\boldsymbol{r}_2-\boldsymbol{\rho}_2)^2\right],
\end{aligned} \tag{8}
$$

where η denotes the twisted factor.

Substituting Equations (5)–(7) into Equation (8), we can obtain the expression of the CSDM for a PCTLGP beam propagating through the anisotropic atmospheric turbulence

$$
\begin{aligned}
W_{\alpha\beta}(\boldsymbol{\rho}_1, \boldsymbol{\rho}_2, L; \omega) = {} & \frac{W_1 W_2 T_0}{8\pi\Omega_0} \frac{\omega^2}{\left(2^{2n+l}cLn!\right)^2} \exp\left[-\frac{(\omega-\omega_0)^2}{\Omega_0^2}\right] \\
& \times \exp\left[-\frac{i\omega}{2cL}\left(\boldsymbol{\rho}_1^2 - \boldsymbol{\rho}_2^2\right)\right] \exp\left[-\frac{1}{\rho_0^2}(\boldsymbol{\rho}_1 - \boldsymbol{\rho}_2)^2\right] \\
& \times \sum_{a_1=0}^{n}\sum_{b_1=0}^{l}\sum_{p_1=0}^{n}\sum_{q_1=0}^{l}\sum_{a_2=0}^{l+2a_1-b_1}\sum_{b_2=0}^{l+2p_1-q_1-a_2}\sum_{p_2=0}^{[a_2/2]}\sum_{q_2=0}^{[(l+2p_1-q_1)/2]}\sum_{a_3=0}^{l+2p_1-q_1+a_2-2p_2-2q_2}\sum_{b_3=0}^{a_3}\sum_{p_3=0}^{[b_3/2]}\sum_{q_3=0}^{[(2n-2a_1+b_1)/2]} \\
& \times \sum_{a_4=0}^{2n-2a_1+b_1+b_3-2p_3-2q_3}\sum_{b_4=0}^{[b_2/2]}\sum_{p_4=0}^{[(a_3-b_3)/2]}\sum_{q_4=0}^{[a_4/2]}\sum_{q_5=0}^{[(2n-2p_1+q_1)/2]} (i^{b_1})^* i^{q_1} \Delta_1 \Delta_2 \Delta_3 \Delta_4 \\
& \times \left(\frac{\omega\eta}{c}\right)^{b_2+a_3-2b_4-2p_3-2p_4} H_{l+2a_1-a_2-b_1-b_2}\left(\frac{\sqrt{2}u_{1x}}{\sqrt{A^2\sigma^2-2A}}\right) H_{l+a_2-a_3+2p_1-q_1-2p_2-2q_2}\left(\frac{\sqrt{2}iE_2}{2\sqrt{E_1}}\right) \\
& \times H_{2n-2a_1-a_4+b_1+b_3-2p_3-2q_3}\left(\frac{\sqrt{2}iM_2}{2\sqrt{E_3}}\right) H_{2n+a_3+a_4+b_2-b_3-2b_4-2p_1+q_1-2p_4-2q_4-2q_5}\left(\frac{iM_4}{2\sqrt{M_3}}\right)
\end{aligned} \tag{9}
$$

with

$$
\left\{
\begin{aligned}
& A = \frac{1}{\sigma^2} + \frac{1}{2\delta^2} + \frac{1}{\rho_0^2} + \frac{i\omega}{2cL}, B = \frac{1}{\delta^2} + \frac{2}{\rho_0^2}, u_{1x} = \frac{i\omega x_1}{cL} - \frac{x_1-x_2}{\rho_0^2}, \\
& u_{1y} = \frac{i\omega y_1}{cL} - \frac{y_1-y_2}{\rho_0^2}, u_{2x} = -\frac{i\omega x_2}{cL} + \frac{x_1-x_2}{\rho_0^2}, u_{2y} = -\frac{i\omega y_2}{cL} + \frac{y_1-y_2}{\rho_0^2}, \\
& E_1 = -\frac{B^2}{4A} + A^*, E_2 = \frac{u_{1x}B}{2A} + u_{2x}, E_3 = \frac{\omega^2\eta^2}{4c^2E_1} + A, \\
& M_1 = \frac{\omega^2\eta^2 B}{4c^2 AE_1} + B, M_2 = \frac{i\omega\eta E_2}{2cE_1} + u_{1y}, M_3 = \frac{\omega^2\eta^2}{4c^2 A} + \frac{\omega^2\eta^2 B^2}{16c^2 A^2 E_1} - \frac{M_1^2}{4E_3} + A^*, \\
& M_4 = -\frac{i\omega\eta u_{1x}}{2cA} - \frac{i\omega\eta BE_2}{4cAE_1} + \frac{M_1 M_2}{2E_3} + u_{2y}, \\
& W_1 = \exp\left(\frac{u_{1x}^2}{4A}\right)\exp\left(\frac{E_2^2}{4E_1}\right)\exp\left(\frac{M_2^2}{4E_3}\right)\exp\left(\frac{M_4^2}{4M_3}\right), \\
& W_2 = \left(\frac{\sqrt{A\sigma^2-2}}{2i\sigma^2}\right)^l \left(\frac{1}{\sqrt{AE_1}}\right)^{l+1}\left(\frac{2}{\sigma^4}\right)^n\left(\frac{1}{\sqrt{E_3 M_3}}\right)^{2n+1}, \\
& \Delta_1 = \binom{n}{a_1}\binom{l}{b_1}\binom{n}{p_1}\binom{l}{q_1}\binom{a_3}{b_3}\binom{l+2a_1-b_1}{a_2}\binom{l+2a_1-b_1-a_2}{b_2} \\
& \quad \times \binom{l+2p_1-q_1+a_2-2p_2-2q_2}{a_3}\binom{2n-2a_1+b_1+b_3-2p_3-2q_3}{a_4}, \\
& \Delta_2 = \frac{a_2!a_4!b_2!b_3!}{b_4!p_2!q_2!p_3!q_3!p_4!q_4!q_5!(a_2-2p_2)!(a_4-2q_4)!(b_2-2b_4)!(b_3-2p_3)!} \\
& \quad \times \frac{(a_3-b_3)!(2n-2p_1+q_1)!(l+2p_1-q_1)!(2n-2a_1+b_1)!}{(a_3-b_3-2p_4)!(2n-2p_1+q_1-2q_5)!(l+2p_1-q_1-2q_2)!(2n-2a_1+b_1-2q_3)!}, \\
& \Delta_3 = \left(\frac{2E_3-\sigma^2 AE_3}{4A}\right)^{a_1}\left(\frac{2\sqrt{A}}{i\sqrt{\sigma^2 AE_3-2E_3}}\right)^{b_1}\left(\frac{M_3}{2E_1}\right)^{p_1}\left(\sqrt{\frac{2E_1}{M_3}}\right)^{q_1} \\
& \quad \times \left(\frac{B}{i\sqrt{A^2 E_1\sigma^2-2AE_1}}\right)^{a_2}\left(-\frac{\sqrt{2}}{\sqrt{\sigma^2 A^2 M_3-2AM_3}}\right)^{b_2}\left(\frac{2A^2 E_1\sigma^2-4AE_1}{B^2}\right)^{p_2}(\sigma^2 E_1)^{q_2}, \\
& \Delta_4 = \left(\frac{B}{2iA\sqrt{2E_1 M_3}}\right)^{a_3}\left(-\frac{A\sqrt{2M_3}}{B\sqrt{E_3}}\right)^{b_3}(2E_1 E_3)^{p_3}(\sigma^2 E_3)^{q_3} \\
& \quad \times \left(\frac{M_1}{\sqrt{2E_3 M_3}}\right)^{a_4}\left(-\frac{\sigma^2 A^2 M_3-2AM_3}{2}\right)^{b_4}\left(\frac{4A^2 E_1 M_3}{B^2}\right)^{p_4}\left(-\frac{2E_3 M_3}{M_1^2}\right)^{q_4}\left(\frac{\sigma^2 M_3}{2}\right)^{q_5}.
\end{aligned}
\right. \tag{10}
$$

In the above derivations, we have used the following formulas [13,20]:

$$H_n(x+y) = \frac{1}{2^{n/2}} \sum_{m=0}^{n} \binom{n}{m} H_m\left(\sqrt{2}x\right) H_{n-m}\left(\sqrt{2}y\right), \tag{11}$$

$$\int_{-\infty}^{\infty} x^n \exp\left[-(x-\gamma)^2\right] dx = (2i)^{-n} \sqrt{\pi} H_n(i\gamma), \tag{12}$$

$$H_n(x) = \sum_{m=0}^{[n/2]} (-1)^m \frac{n!}{m!(n-2m)!} (2x)^{n-2m}, \tag{13}$$

$$\int_{-\infty}^{\infty} \exp\left[-(x-y)^2\right] H_n(mx) dx = \sqrt{\pi} \left(1-m^2\right)^{n/2} H_n\left[\frac{my}{(1-m^2)^{1/2}}\right]. \tag{14}$$

The spectral density along the observation plane at the "coincident point" $\rho_1 = \rho_2 = \rho = (x, y)$ is given by the formula [7,9,13]:

$$S(\rho, L; \omega) = W_{xx}(\rho, \rho, L; \omega) + W_{yy}(\rho, \rho, L; \omega). \tag{15}$$

According to Equations (9), (10) and (15), the spectral density of a PCTLGP beam is mainly determined by the twisted factor η, topological charge l, mode order n, pulse duration T_0 and turbulence parameters.

3. Numerical Simulation and Discussion

In this section, we numerically calculate the spectral intensity of the PCTLGP beam propagating through the anisotropic non-Kolmogorov turbulence by using the above analyses. The parameters in the following calculations were set as $\lambda = 1550$ nm, $\sigma = 20$ mm, $\delta = 10$ mm, $\omega_0 = 2.9788$ rad/fs, $\omega = 1.02\omega_0$, $T_0 = 100$ fs, $T_c = 50$ fs, $\alpha = 3.4$, $L_0 = 50$ m, $l_0 = 10$ mm; the other parameters were specified in the figure captions.

To understand the twist phase induced evolution of the spectral intensity distribution on propagation, Figure 1 shows both the 3D-normalized spectral intensity distribution of the PCLGP beam ($\eta = 0$ m^{-1}) and the PCTLGP beam ($\eta = -5 \times 10^{-4}$ m^{-1}) at several propagation distances in anisotropic non-Kolmogorov turbulence. In Figure 1(a1,b1), one finds that the initial beam profiles of the PCLGP beam and the PCTLGP beam show a multi-ring dark hollow beam profile. From Figure 1(a1–a8), the evolution process of the PCLGP beam can be seen: the spectral intensity in the dark center region gradually increases with the increase in the propagation distance, and the dark ring gradually disappears, and the outer ring gradually degenerates, and finally the beam spot evolves into a Gaussian shape. Similarly, for a PCTLGP beam (see Figure 1(b1–b8)), the spectral intensity distribution gradually evolves to a flat-top distribution, and eventually converges into a Gaussian-like distribution. This is consistent with the conclusions in Refs. [15,31–33]: The Kurtosis parameters of the arbitrary beams will converge to a constant 2 as the propagation distance $L \to \infty$, which means that arbitrary beams will evolve into a Gaussian shape in atmospheric turbulence with the increase in L. Compared to Figure 1a,b, it can be found that the PCLGP beam evolves into Gaussian distribution more quickly than the PCTLGP beam during transmission, which indicates that the twist phase plays an important role in resistance to the turbulence-induced degeneration.

Next, we focus on the influence of the topological charge on the evolution properties during propagation. Figure 2 shows the normalized spectral intensity distribution of the PCTLGP beam propagating through the anisotropic non-Kolmogorov turbulence ($\widetilde{C}_n^2 = 1 \times 10^{-17}$ m$^{3-\alpha}$) at several propagation distances for the different topological charges. Figure 2a,c,d presents that the normalized spectral intensity distribution of the PCTLGP beam gradually evolves from a dark hollow distribution to a flat-topped distribution when $n = 0$, and finally converges into a Gaussian-like distribution. Figure 2b displays the normalized spectral intensity distribution of the PCTLGP beam when $n \neq 0$, and the results shown agree with those discussed in Figure 1. Importantly, we find that the evolution of

the PCTLGP beam can be accelerated with the decrease in *l*, indicating that the PCTLGP beam with a larger *l* has a stronger ability to resist the degeneration caused by the turbulent atmosphere. In Ref. [14], the partially coherent radially polarized vortex beam studied by Yu et.al. also showed a similar phenomenon. Furthermore, it can be seen that the progress of the beam evolving into a Gaussian-like shape will not be accelerated with the increase in the propagation distance when it propagates for a long distance (*L* > 3 km), which is caused by the too weak turbulence, but the beam spot is larger with the increase in *L*.
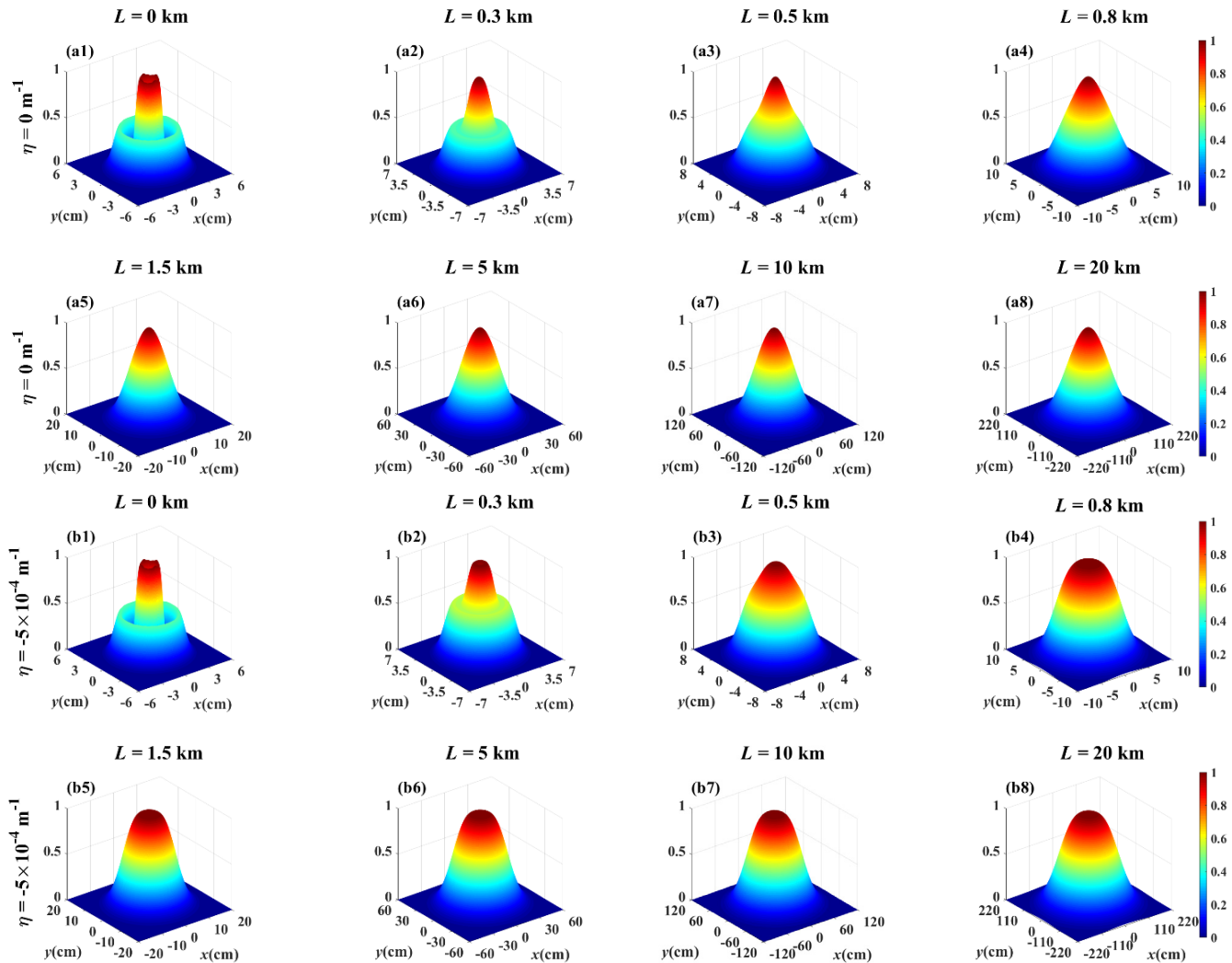
Figure 1. Normalized spectral intensity distribution of (**a1**–**a8**) the PCLGP beam and (**b1**–**b8**) the PCTLGP beam at several propagation distances in anisotropic turbulence ($\xi_x = \xi_y = 3$, $l = 1$, $n = 1$, $\widetilde{C}_n^2 = 1 \times 10^{-14}$ m$^{3-\alpha}$).

For comparison, Figure 3 depicts the normalized spectral intensity distribution of the PCTLGP beam propagating through the anisotropic non-Kolmogorov turbulence ($\widetilde{C}_n^2 = 1 \times 10^{-13}$ m$^{3-\alpha}$) at the same propagation distances and the topological charges with Figure 2. Figure 3a–d shows the progress of the normalized spectral intensity distribution for the PCTLGP beam gradually evolves to a Gaussian-like distribution under different mode orders and topological charges. It can be easily found that the degeneration of the PCTLGP beam is accelerated by the stronger turbulence by comparing Figures 2 and 3. It is also found that the PCTLGP beam shows different evolution properties when propagating in weaker turbulence and stronger turbulence. The degradation progress of the beam is accelerated with increasing *L* when propagating for *L* > 3 km in stronger atmospheric turbulence, and it eventually converges to a Gaussian-like distribution, while the

weakly turbulent atmosphere has little effect on the progress of the beam evolving into a Gaussian-like shape, and only the beam spot becomes lager with the increase in *L*.
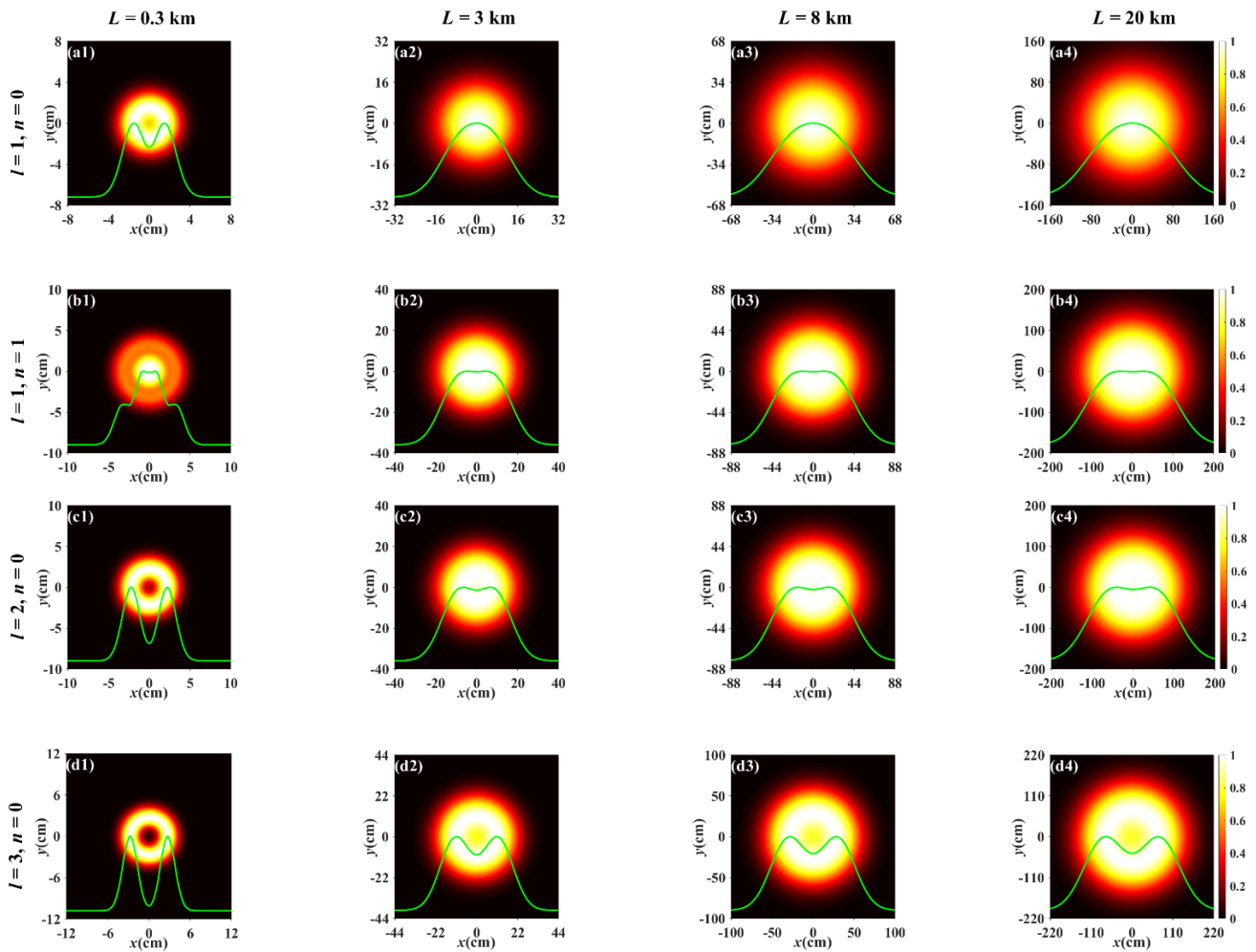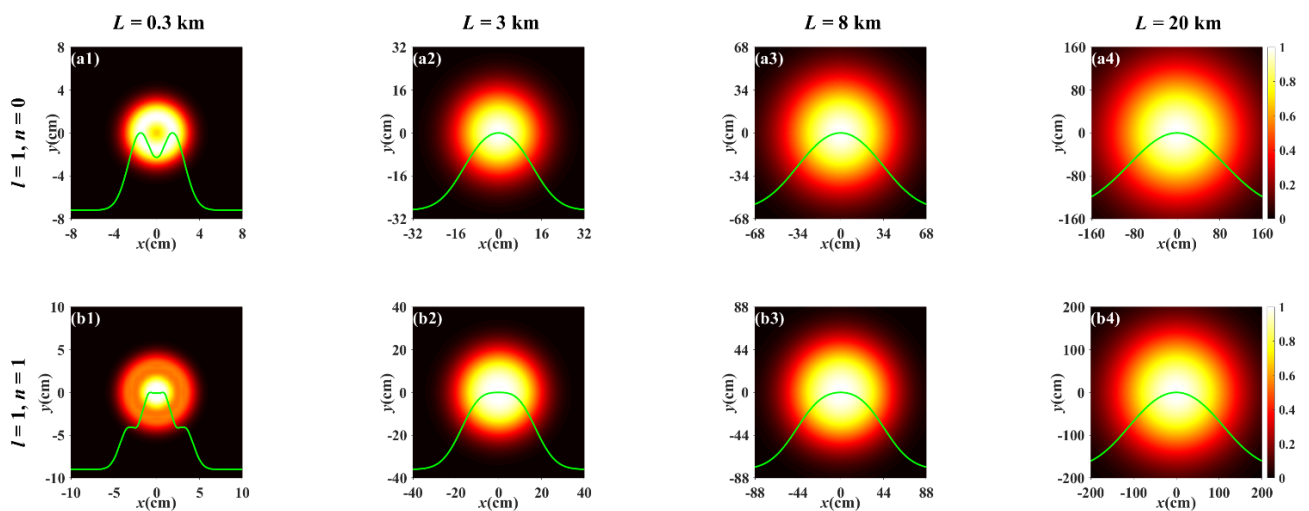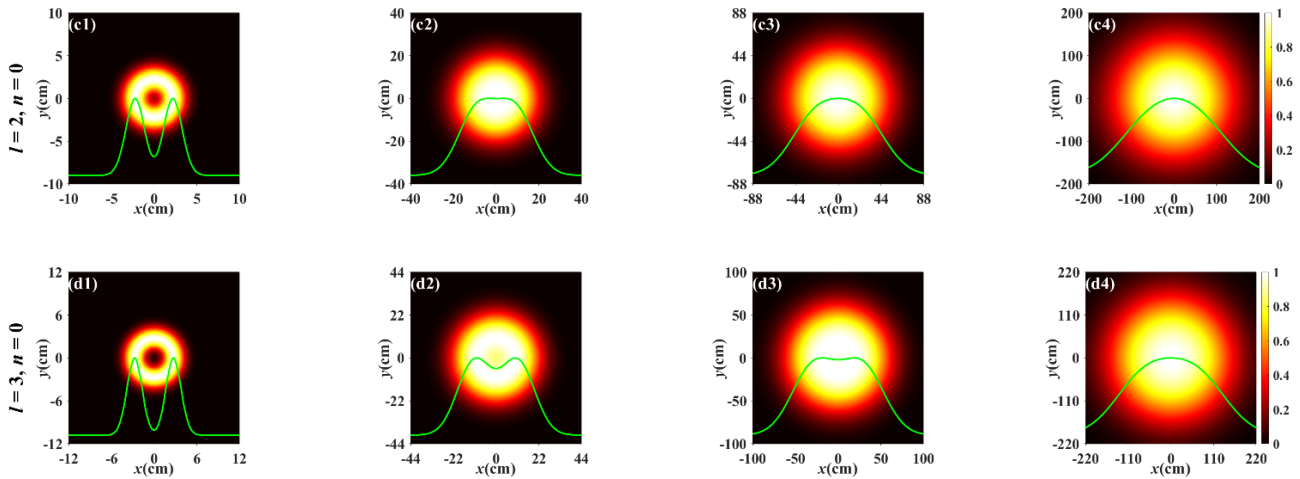

Figure 2. Normalized spectral intensity distribution of the PCTLGP beam at several propagation distances in anisotropic turbulence for different mode orders and topological charges ($\xi_x = \xi_y = 3$, $\widetilde{C}_n^2 = 1 \times 10^{-17}$ m$^{3-\alpha}$, $\eta = -5 \times 10^{-4}$ m^{-1}).

Figure 3. *Cont.*

Figure 3. Normalized spectral intensity distribution of the PCTLGP beam at several propagation distances in anisotropic turbulence for different mode orders and topological charges ($\xi_x = \xi_y = 3$, $\widetilde{C}_n^2 = 1 \times 10^{-13}$ m$^{3-\alpha}$, $\eta = -5 \times 10^{-4}$ m^{-1}).

To explore the influence of the twisted factor on the evolution of the beam, Figure 4 studies the normalized spectral intensity distribution of the PCTLGP beam with $\eta = -1 \times 10^{-3}$ m^{-1} propagating through the weaker turbulence ($\widetilde{C}_n^2 = 1 \times 10^{-17}$ m$^{3-\alpha}$). Figure 4a–d illustrates the evolution of the PCTLGP beam in the turbulent atmosphere, and it can be seen that the degeneration of the PCTLGP beam will be suppressed with the increase in l. Compared to Figures 2 and 4, it can be found that the PCTLGP beam with the smaller η has a stronger ability to maintain the dark hollow distribution when propagating in the weaker turbulence, meaning that the PCTLGP beam has an advantage over the PCLGP beam for resisting the degeneration caused by turbulence, and the advantage is further enhanced with decreasing η.
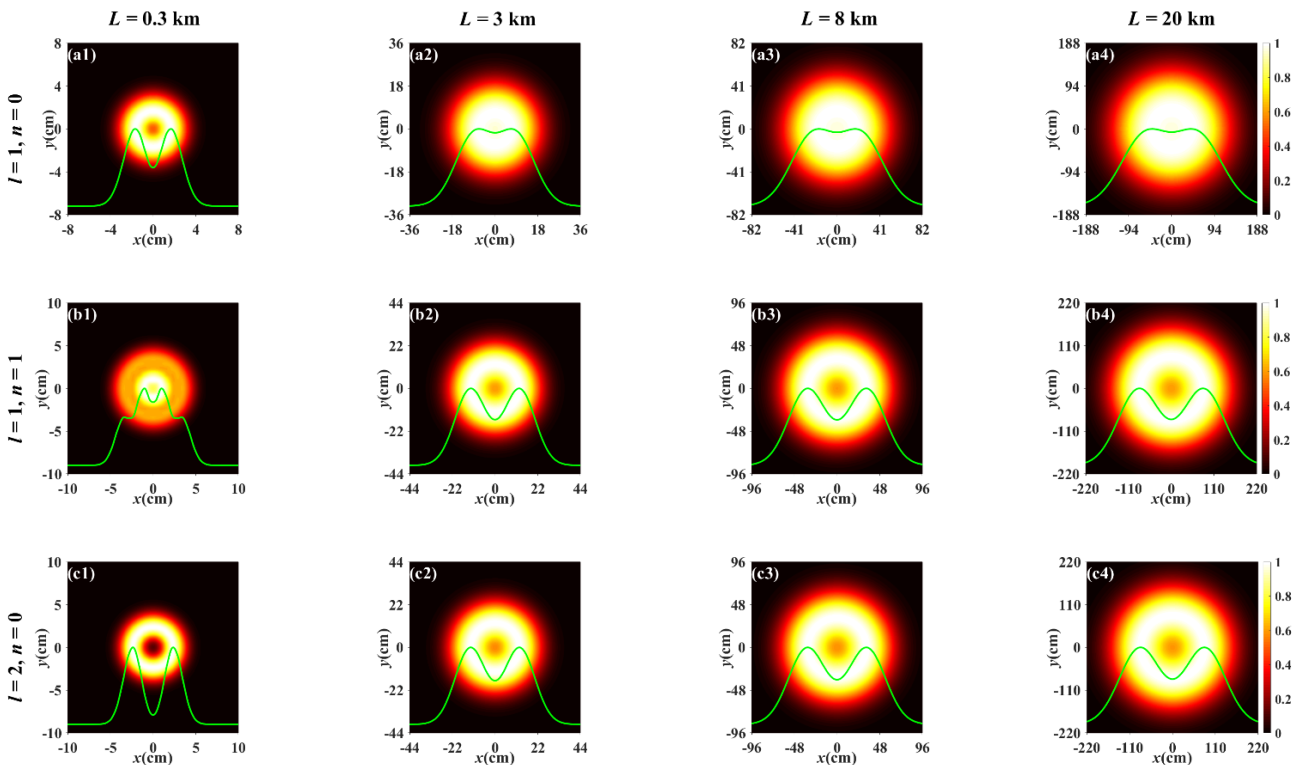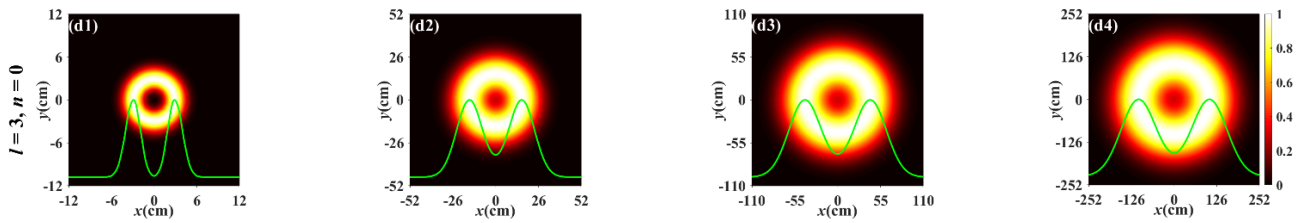

Figure 4. *Cont.*

Figure 4. Normalized spectral intensity distribution of the PCTLGP beam at several propagation distances in anisotropic turbulence for different mode orders and topological charges ($\xi_x = \xi_y = 3$, $\widetilde{C}_n^2 = 1 \times 10^{-17}$ m$^{3-\alpha}$, $\eta = -1 \times 10^{-3}$ m^{-1}).

Figure 5 illustrates the evolution of the normalized spectral intensity distribution for a PCTLGP beam with $\eta = -1 \times 10^{-3}$ m^{-1} propagating through the stronger turbulence ($\widetilde{C}_n^2 = 1 \times 10^{-13}$ m$^{3-\alpha}$). Figure 5a–d depicts the degeneration of the PCTLGP beam with different l and n in the turbulent atmosphere. Compared to Figures 3 and 5, it can be seen that the above conclusions obtained from comparing Figures 2 and 4 are also applicable to the stronger turbulence, that is to say, whether in stronger turbulence or weaker turbulence, the PCTLGP beam with a smaller η can more effectively resist the influence of the turbulence on the degeneration. Next, we focus on the effect of the joint modulation of the twist factor and the topological charge on the beam evolution.
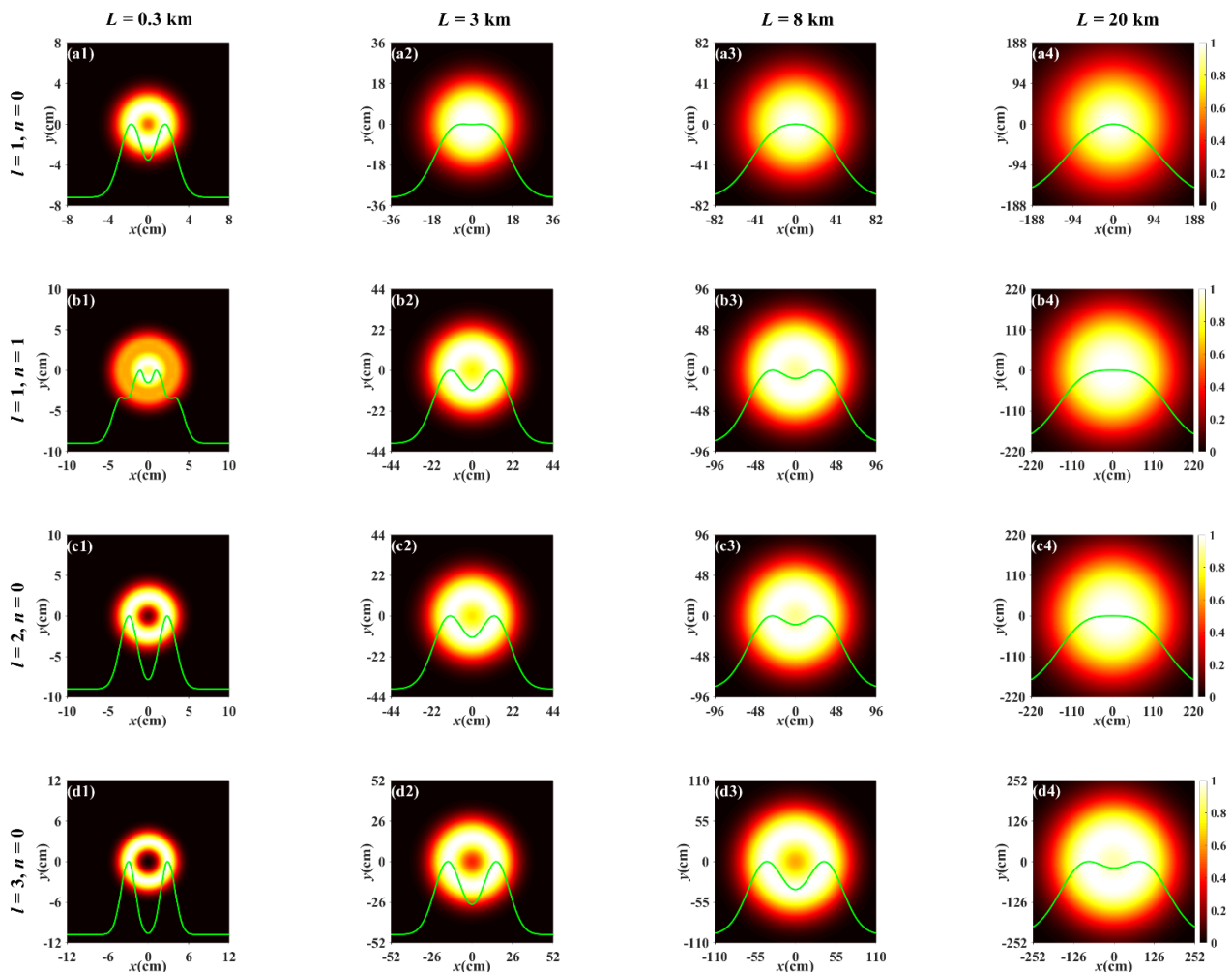

Figure 5. Normalized spectral intensity distribution of the PCTLGP beam at several propagation distances in anisotropic turbulence for different mode orders and topological charges ($\xi_x = \xi_y = 3$, $\widetilde{C}_n^2 = 1 \times 10^{-13}$ m$^{3-\alpha}$, $\eta = -1 \times 10^{-3}$ m^{-1}).

Figure 6 gives the evolution of the normalized spectral intensity distribution of the PCTLGP beam on propagation through anisotropic non-Kolmogorov turbulent atmosphere for the different topological charges and twisted factors. Figure 6a–c studies the influence of the sign of the twisted factor on the beam evolution, and the results present that the process of the beam evolving into a Gaussian shape is accelerated by modulating the sign of twisted factor is "+". Conversely, the evolution process is suppressed when the sign is "−". In addition, Figure 6c,d shows that the values of l and η will affect the degeneration of the PCTLGP beam, and one finds that the beam degenerates more slowly when both l and $|\eta|$ are larger, which means that the PCTLGP beam with a negative twisted factor shows an advantage in resisting the turbulence-induced degeneration, and this advantage is further enhanced with increasing l and $|\eta|$.
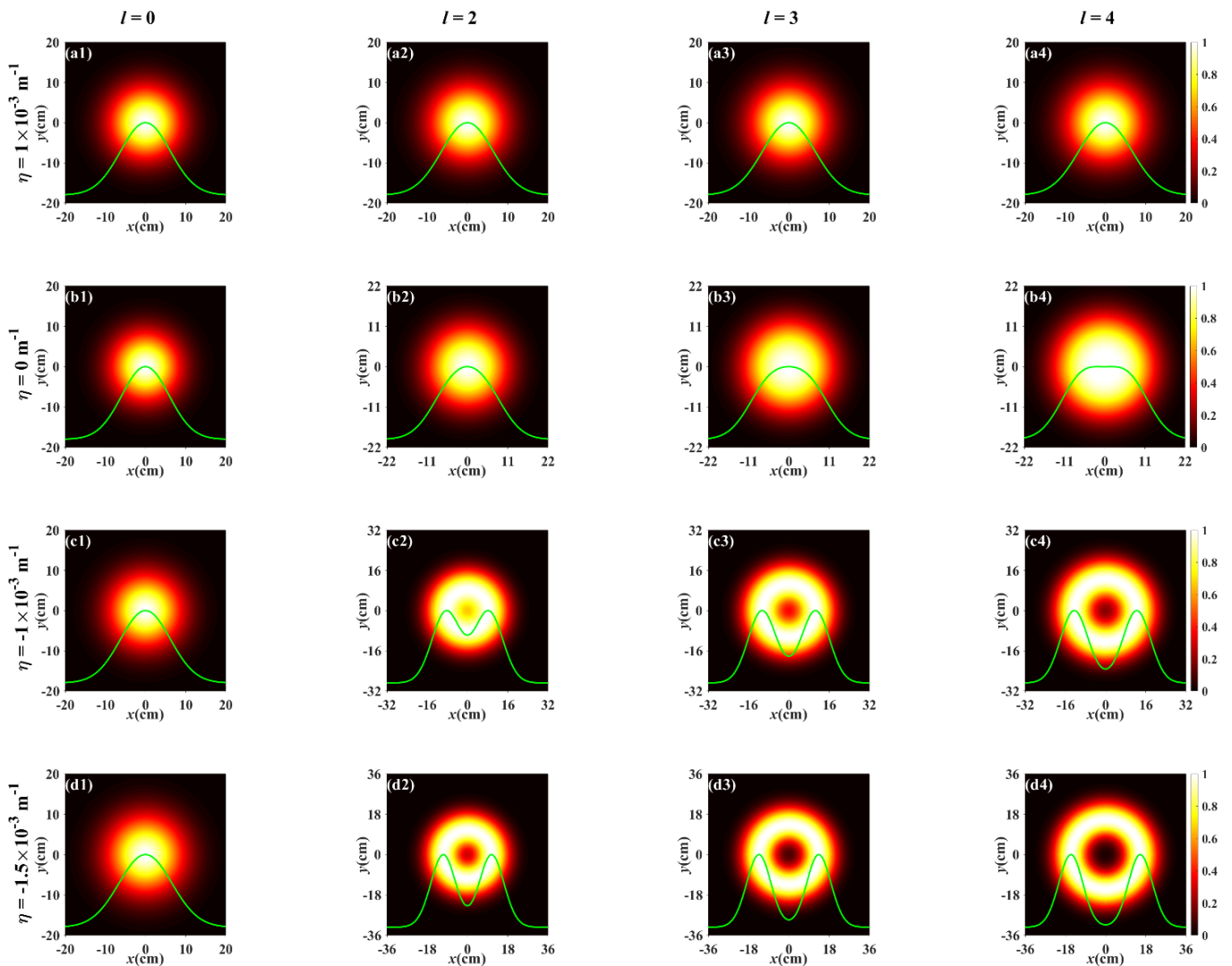

Figure 6. Normalized spectral intensity distribution of the PCTLGP beam propagating through the anisotropic turbulence for different twisted factors and topological charges ($\widetilde{C}_n^2 = 5 \times 10^{-14}$ m$^{3-\alpha}$, $\xi_x = \xi_y = 2$, $L = 2$ km, $n = 0$).

For comparison, we introduce the normalized spectral intensity $S(T_0) = S(\boldsymbol{\rho}, L; \omega)/S_{\max}(\boldsymbol{\rho}, L; \omega)$, where $S_{\max}(\boldsymbol{\rho}, L; \omega)$ is the maximum spectral intensity at the points $\boldsymbol{\rho} = (x, y)$ when the pulse duration is 100 fs. Figure 7 illustrates the $S(T_0)$ of the PCTLGP beam propagating for 0.3 km in anisotropic non-Kolmogorov turbulent atmosphere under the different pulse durations. Obviously, Figure 7 shows that the overall $S(T_0)$ increases with increasing T_0. Figure 7a–c illustrates the influence of the twisted factor, the topological charge and the mode order on $S(T_0)$, respectively. It can be found that the ability of the

PCTLGP beam to maintain the dark hollow shape is enhanced with increasing *l*, and the dark ring of the beam is more obvious when *n* is larger. Moreover, the PCTLGP beam degrades more slowly when the sign of the twisted factor is "−". Therefore, we can draw a conclusion: the PCTLGP beam with a negative twisted factor can more effectively resist the influence of turbulence, and this resistance ability is further enhanced with increasing *l*, *n*.
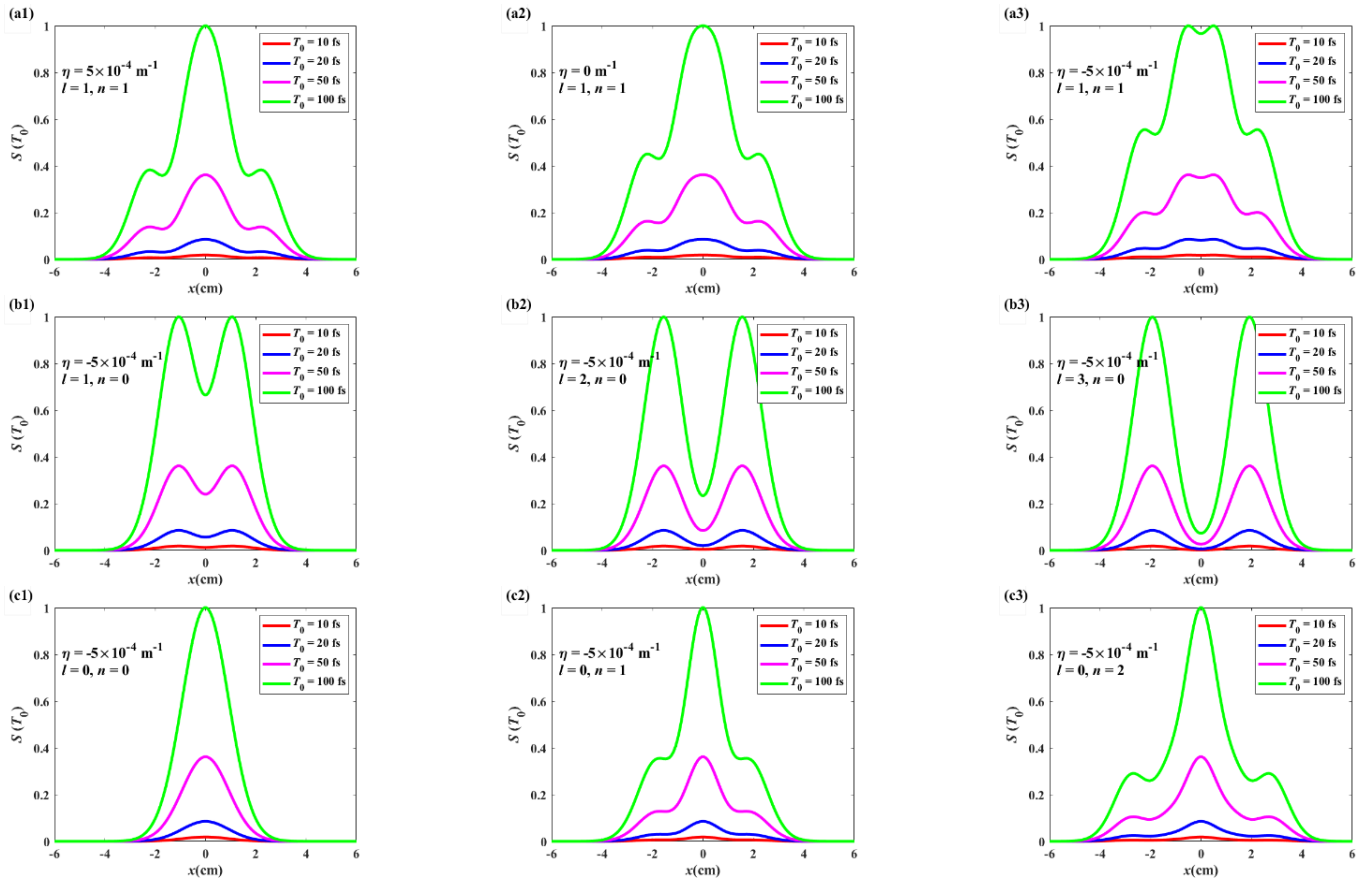

Figure 7. The relationship between the normalized spectral intensity with pulse duration of the PCTLGP beam propagating through the anisotropic turbulence for different (**a1**–**a3**) twisted factors, (**b1**–**b3**) topological charges, (**c1**–**c3**) mode orders ($\xi_x = \xi_y = 3$, $L = 0.3$ km, $\widetilde{C}_n^2 = 1 \times 10^{-14}$ m$^{3-\alpha}$).

4. Conclusions

In this paper, we have derived the analytical expressions for the diagonal elements of the CSDM for a PCTLGP beam in anisotropic turbulent atmosphere. The evolution properties of the PCTLGP beam on propagation are numerically discussed in detail. It is found that the initial beam profile of the PCTLGP beam ($n \neq 0$) shows a multi-ring dark hollow beam profile, and it will degenerate into a flat-top distribution with the increase in the propagation distance and eventually evolves into a Gaussian-like distribution in the far field. In addition, the influence of the twisted factor η, topological charge *l*, mode order *n*, pulse duration T_0 and turbulence parameters on the spectral intensity of the PCTLGP beam propagating through the turbulent atmosphere have been studied, and we find the most important parameters affecting the spectral intensity are the twisted factor η and topological charge *l*. Numerical results show that the PCTLGP beam with a negative twisted factor shows an advantage over the PCLGP beam in resisting the turbulence-induced degeneration, and this advantage is further strengthened with increasing *l* and $|\eta|$. Moreover, the ability of the PCTLGP beam to resist turbulence also increases with the increase in *n*, and the pulse duration will affect the value of the spectral intensity, which increases with increasing T_0. It is also found that the PCTLGP beam shows different evolution properties when propagating in weaker turbulence and stronger turbulence.

When the PCTLGP beam propagates for long distances in a weakly turbulent atmosphere, the progress of the beam evolving into a Gaussian-like shape will not be accelerated with the increase in the propagation distance, and only the beam spot will become lager. However, the degradation progress of the beam is accelerated with increasing *L* when propagating for long distances in stronger atmospheric turbulence, and it eventually converges to the Gaussian-like distribution. Compared with the general PCLGP beam, the PCTLGP beam shows some advantages. Therefore, the PCTLGP beam will be useful in free-space optical communications and remote sensing.

Institutional Review Board Statement: Not applicable.

Informed Consent Statement: Not applicable.

Data Availability Statement: Exclude this statement.

Conflicts of Interest: The authors declare no conflict of interest.

References

1. Paakkonen, P.; Turunen, J.; Vahimaa, P.; Friberg, A.; Wyrowski, F. Partially coherent Gaussian pulses. *Opt. Commun.* **2002**, *204*, 53–58. [CrossRef]
2. Lin, Q.; Wang, L.; Zhu, S. Partially coherent light pulse and its propagation. *Opt. Commun.* **2003**, *219*, 65–70. [CrossRef]
3. Liu, D.; Wang, Y.; Wang, G.; Yin, H.; Wang, J. The influence of oceanic turbulence on the spectral properties of chirped Gaussian pulsed beam. *Opt. Laser Technol.* **2016**, *82*, 76–81. [CrossRef]
4. Ding, C.; Korotkova, O.; Horoshko, D.; Zhao, Z.; Pan, L. Evolution of Spatiotemporal Intensity of Partially Coherent Pulsed Beams with Spatial Cosine-Gaussian and Temporal Laguerre-Gaussian Correlations in Still, Pure Water. *Photonics* **2021**, *8*, 102. [CrossRef]
5. Wang, H.; Yan, X.; Feng, X.; Zhao, Z.; Pan, L. Intensity Evolution of Cosine-Gaussian-Correlated Schell-Model Pulse Scattered by a Medium. *Appl. Sci.* **2020**, *10*, 1825. [CrossRef]
6. Liu, D.; Luo, X.; Wang, G.; Wang, Y. Spectral and Coherence Properties of Spectrally Partially Coherent Gaussian Schell-model Pulsed Beams Propagating in Turbulent Atmosphere. *Curr. Opt. Photonics* **2017**, *1*, 271–277.
7. Li, Y.; Gao, M.; Lv, H.; Wang, L.; Ren, S.; Hu, X. Anisotropic turbulence-induced statistical properties evolution of a radially polarized partially coherent pulsed beam on propagation. *Opt. Commun.* **2020**, *466*, 125669. [CrossRef]
8. Wang, X.; Tang, J.; Wang, Y.; Liu, X.; Liang, C.; Zhao, L.; Hoenders, B.; Cai, Y.; Ma, P. Complex and phase screen methods for studying arbitrary genuine Schell-model partially coherent pulses in nonlinear media. *Opt. Express* **2022**, *30*, 24222–24231. [CrossRef]
9. Li, Y.; Gao, M.; Li, B. Vortex phase induced evolution of propagation properties of a spatiotemporally partially coherent partially polarized pulsed beam in atmospheric turbulence. *Opt. Commun.* **2022**, *518*, 128385. [CrossRef]
10. Zhao, J.; Wang, G.; Ma, X.; Zhong, H.; Yin, H.; Wang, Y.; Liu, D. Intensity and Coherence Characteristics of a Radial Phase-Locked Multi-Gaussian Schell-Model Vortex Beam Array in Atmospheric Turbulence. *Photonics* **2021**, *8*, 5. [CrossRef]
11. Guo, Z. Coherent Property Evolution of Partially Coherent Elliptical Vortex Beam Propagation Through Turbulence. *Laser Optoelectron. Prog.* **2021**, *58*, 0901001.
12. Liu, D.; Wang, Y.; Wang, G.; Yin, H. Propagation properties of a partially coherent anomalous hollow vortex beam in uniaxial crystal orthogonal to the optical axis. *J. Mod. Opt.* **2018**, *65*, 1442–1449. [CrossRef]
13. Xu, Y.; Zhao, L.; Yang, N.; Xu, Y. Propagation characteristics of partially coherent twisted Laguerre-Gaussian beam in atmospheric turbulence with anisotropy. *J. Mod. Opt.* **2022**, *69*, 200–209. [CrossRef]
14. Yu, J.; Huang, Y.; Wang, F.; Liu, X.; Gbur, R.; Cai, Y. Scintillation properties of a partially coherent vector beam with vortex phase in turbulent atmosphere. *Opt. Express* **2019**, *27*, 26676–26688. [CrossRef]
15. Zhao, L.; Xu, Y.; Dan, Y. Evolution properties of partially coherent radially polarized Laguerre-Gaussian vortex beams in an anisotropic turbulent atmosphere. *Opt. Express* **2021**, *29*, 34986–35002. [CrossRef]
16. Peng, X.; Liu, L.; Wang, F.; Popov, S.; Cai, Y. Twisted Laguerre-Gaussian Schell-model beam and its orbital angular moment. *Opt. Express* **2018**, *26*, 33956–33969. [CrossRef]

17. Zhong, W.; Yang, Z.; Belic, M.; Zhong, W. Two-dimensional asymmetric Laguerre-Gaussian diffraction-free beams. *Phys. Lett. A* **2022**, *423*, 127818. [CrossRef]

18. Zhong, W.P.; Zhong, W.; Belic, M.; Yang, Z. Controllable two-dimensional diffraction-free polygon beams. *Phys. Lett. A* **2022**, *432*, 128009. [CrossRef]

19. Pan, X.; Wu, J.; Li, Z.; Zhang, C.; Deng, C.; Zhang, Z.; Wen, H.; Gao, Q.; Yang, J.; Yi, Z.; et al. Laguerre-Gaussian mode purity of Gaussian vortex beams. *Optik* **2021**, *230*, 166320. [CrossRef]

20. Xu, Y.; Li, Y.; Zhao, X. Intensity and effective beam width of partially coherent Laguerre–Gaussian beams through a turbulent atmosphere. *J. Opt. Soc. Am. A* **2015**, *32*, 1623–1630. [CrossRef]

21. Martínez-Matos, Ó.; Vaveliuk, P.; Izquierdo, J.; Loriot, V. Femtosecond spatial pulse shaping at the focal plane. *Opt. Express* **2013**, *21*, 25010–25025. [CrossRef] [PubMed]

22. Liu, Y.; Gao, C. Study on the time-varying and propagating characteristics of ultrashort pulse Laguerre-Gaussian beam. *Opt. Express* **2010**, *18*, 12104–12110. [CrossRef] [PubMed]

23. Li, Y.; Zhang, Y.; Zhu, Y. Probability distribution of the orbital angular momentum mode of the ultrashort Laguerre-Gaussian pulsed beam propagation in oceanic turbulence. *Results Phys.* **2018**, *11*, 698–705. [CrossRef]

24. Liu, Z.; Wan, L.; Zhou, Y.; Zhang, Y.; Zhao, D. Progress on Studies of Beams Carrying Twist. *Photonics* **2021**, *8*, 92. [CrossRef]

25. Zhou, Y.; Zhao, D. Propagation properties of a twisted rectangular multi-Gaussian Schell-model beam in free space and oceanic turbulence. *Appl. Opt.* **2018**, *57*, 8978–8983. [CrossRef]

26. Cui, Y.; Wang, F.; Cai, Y. Propagation of a twist Gaussian-Schell model beam in non-Kolmogorov turbulence. *Opt. Commun.* **2014**, *324*, 108–113. [CrossRef]

27. Zhao, Y.; Liu, X.; Liang, C.; Liu, L.; Wang, F.; Cai, Y. Statistical Characteristics of a Twisted Anisotropic Gaussian Schell-Model Beam in Turbulent Ocean. *Photonics* **2020**, *7*, 37.

28. Liu, Y.; Lin, R.; Wang, F.; Cai, Y.; Yu, J. Propagation properties of Laguerre-Gaussian Schell-model beams with a twist phase. *J. Quant. Spectrosc. Radiat. Transf.* **2021**, *264*, 107556. [CrossRef]

29. Zhang, B.; Huang, H.; Xie, C.; Zhu, S.; Li, Z. Twisted rectangular Laguerre-Gaussian correlated sources in anisotropic turbulent atmosphere. *Opt. Commun.* **2020**, *459*, 125004. [CrossRef]

30. Madhu, V.; Ivan, J. Robustness of the twist parameter of Laguerre-Gaussian mode superpositions against atmospheric turbulence. *Phys. Rev. A* **2017**, *95*, 043836.

31. Xu, Y.; Dan, Y.; Yu, J.; Cai, Y. Kurtosis parameter K of arbitrary electromagnetic beams propagating through non-Kolmogorov turbulence. *J. Mod. Opt.* **2017**, *64*, 1976–1987. [CrossRef]

32. Xu, Y.; Xu, Y.; Wang, S.; Deng, X.; Liu, Y.; Wang, S. Kurtosis parameter and coupling coefficient of partially-coherent twisted Gaussian beam propagating through non-Kolmogorov atmospheric turbulence. *J. Russ. Laser Res.* **2022**, *43*, 509–519. [CrossRef]

33. Zhou, Y.; Cheng, K.; Zhu, B.; Yao, N.; Zhong, X. Beam spreading, kurtosis parameter and Strehl ratio of partially coherent cosh-Airy beams in atmospheric turbulence. *Optik* **2019**, *183*, 656–663. [CrossRef]